Spontaneous IPSCs and glycine receptors with slow kinetics in wide-field amacrine cells in the mature rat retina

Margaret Lin Veruki, Silje Bakken Gill and Espen Hartveit

University of Bergen, Department of Biomedicine, Bergen, Norway

The functional properties of glycine receptors were analysed in different types of wide-field amacrine cells, narrowly stratifying cells considered to play a role in larger-scale integration across the retina. The patch-clamp technique was used to record spontaneous IPSCs (spIPSCs) and glycine-evoked patch responses from mature rat retinal slices (4–7 weeks postnatal). Glycinergic spIPSCs were blocked reversibly by strychnine (300 nM). Compared to previously described spIPSCs in AII amacrine cells, the spIPSCs in wide-field amacrine cells displayed a very slow decay time course ($\tau_{fast} \sim 15$ ms; $\tau_{slow} \sim 57$ ms). The kinetic properties of spIPSCs in whole-cell recordings were paralleled by even slower deactivation kinetics of responses evoked by brief pulses of glycine (3 mM) to outside-out patches from wide-field amacrine cells ($\tau_{fast} \sim 45$ ms; $\tau_{slow} \sim 350$ ms). Non-stationary noise analysis of patch responses and spIPSCs yielded similar average single-channel conductances (∼31 and ∼34 pS, respectively). Similar, as well as both lower- and higher-conductance levels could be identified from directly observed single-channel gating during the decay phase of spIPSCs and patch responses. These results suggest that the slow glycinergic spIPSCs in wide-field amacrine cells involve $\alpha 2\beta$ heteromeric receptors. Taken together with previous work, the kinetic properties of glycine receptors in different types of amacrine cells display a considerable range that is probably a direct consequence of differential expression of receptor subunits. Unique kinetic properties are likely to differentially shape the glycinergic input to different types of amacrine cells and thereby contribute to distinct integrative properties among these cells.

(Received 26 December 2006; accepted after revision 27 February 2007; first published online 1 March 2007)
Corresponding author E. Hartveit: University of Bergen, Department of Biomedicine, Jonas Lies vei 91, N-5009 Bergen, Norway. Email: espen.hartveit@biomed.uib.no

Glycine is an important inhibitory neurotransmitter in spinal cord, brain stem and retina. In the mammalian retina, glycine is employed as a neurotransmitter in ∼50% of all amacrine cells (Pourcho & Goebel, 1985; Menger *et al.* 1998; reviewed by Slaughter, 2004). Amacrine cells are local circuit interneurons that receive synaptic input from bipolar cells and other amacrine cells and send output to bipolar cells, ganglion cells and other amacrine cells. Glycine activates receptors with an integral chloride-selective ion channel. Molecular biological studies have revealed the existence of five different receptor subunits ($\alpha 1$–$\alpha 4$ and β; reviewed by Lynch, 2004). A functional glycine receptor is a pentameric receptor, either an α homomeric receptor or an $\alpha\beta$ heteromeric receptor. Depending on the exact subunit composition, glycine receptors display marked functional variability, including differences in kinetic properties and single-channel conductance (reviewed by Legendre, 2001). The most striking example of the functional consequences of differential expression of glycine receptor subunits is the developmental speeding of glycinergic synaptic transmission in the spinal cord and brain stem (Takahashi *et al.* 1992; Singer *et al.* 1998). The change from slowly to rapidly decaying synaptic responses is accompanied by a change in glycine receptor subunit expression from slow $\alpha 2$ receptors (homomeric $\alpha 2$ or heteromeric $\alpha 2\beta$ receptors) to fast $\alpha 1\beta$ heteromeric receptor channels (Becker *et al.* 1988; Takahashi *et al.* 1992). The $\alpha 2$-subunit is therefore considered an embryonic and juvenile subunit, and at most a minor constituent of glycine receptors in the mature spinal cord and brain stem (Legendre, 2001; Lynch, 2004). The change in receptor expression and synaptic kinetics is considered to play a critical role in the maturation of motor functions (reviewed by Takahashi, 2005). The $\alpha 3$-subunit has a similar developmental expression pattern to that of the $\alpha 1$-subunit, but at all developmental stages the $\alpha 3$-subunit expression level is less intense (Malosio *et al.* 1991). The $\alpha 4$-subunit is expressed in embryonic spinal cord, sympathetic and dorsal root ganglia, but not in the adult brain and spinal cord (Harvey *et al.* 2000).

 DOI: 10.1113/jphysiol.2006.127316

The status of the α2-subunit as an embryonic receptor in the spinal cord and brain stem contrasts with the patterns of expression observed in the adult mammalian retina. As for adult spinal cord and brain stem, there is strong evidence for expression of the α1-subunit (Grünert & Wässle, 1993). In addition, however, immunocytochemical experiments have detected the presence of α2-, α3- and α4-subunits in mature retinal tissue, with strong evidence for a differential expression of these subunits among retinal neurons (Grünert & Wässle, 1993; Haverkamp *et al.* 2003, 2004; Heinze *et al.* 2006). This raises the question whether there might be a corresponding variation of functional properties of retinal glycine receptors. Mammalian retinas contain ∼55 separate neuronal types and it is generally considered that each type, as defined by morphological criteria, carries out a specific physiological function (Masland, 2001). For amacrine cells, ∼30 different types have been distinguished. It has been suggested that amacrine cells only express glycine receptors with slow kinetic properties (Frech *et al.* 2001). However, a recent investigation of AII amacrine cells found evidence for very fast decay kinetics of glycine receptor currents in these cells, both for synaptic currents and for currents evoked in outside-out patches (Gill *et al.* 2006). Here, we have investigated the functional characteristics of glycine receptors in wide-field amacrine cells. These cells display common morphological characteristics with long, radiating processes that stratify narrowly at different levels of the inner plexiform layer (Perry & Walker, 1980; Famiglietti, 1992*a*,*b*; MacNeil & Masland, 1998; MacNeil *et al.* 1999; Völgyi *et al.* 2001; Badea & Nathans, 2004; Lin & Masland, 2006). As a group, wide-field amacrine cells are generally considered to play a role in larger-scale integration across the retina, with each type transmitting inhibition over long distances (reviewed by Baccus, 2007). In the wide-field amacrine cells we recorded from, spontaneous inhibitory postsynaptic currents (spIPSCs) displayed very slow decay kinetics. Importantly, this was parallelled by even slower deactivation kinetics of glycine-evoked responses measured in outside-out patches. This suggested that the slow time course of the spIPSCs is a consequence of the kinetic properties of the glycine receptors expressed by wide-field amacrine cells. A comparison of the present results for wide-field amacrine cells with those obtained previously for AII amacrine cells suggests that unique glycine receptor properties may differentially shape glycinergic input to different types of amacrine cells.

Methods

General aspects of the methods have previously been described in detail (Hartveit, 1996; Veruki *et al.* 2003). Albino rats (4–7 weeks postnatal) were deeply anaesthetized with halothane in oxygen and killed by cervical dislocation (procedure approved under the surveillance of the Norwegian Animal Research Authority). Retinal slices were visualized with a ×40 water immersion objective and infrared differential interference contrast videomicroscopy. When filled with intracellular solution, recording pipettes typically had resistances of 4–6 MΩ for recordings in the whole-cell configuration and 5–8 MΩ for recordings in the outside-out patch configuration. All patches were isolated from the soma of the recorded cells. For some outside-out recordings, pipettes were coated with dental wax and fire-polished immediately before use. Recordings were carried out at room temperature (20–23°C).

Solutions and drugs

The extracellular perfusing solution was continuously bubbled with 95% O_2–5% CO_2 and had the following composition (mM): 125 NaCl, 25 $NaHCO_3$, 2.5 KCl, 2.5 $CaCl_2$, 1 $MgCl_2$, 10 glucose, pH 7.4. The recording pipettes (whole-cell and patch) were filled with (mM): 130 KCl, 10 Hepes, 1 $CaCl_2$, 8 NaCl, 5 EGTA, 4 MgATP, 2 *N*-(2,6-dimethylphenylcarbamoylmethyl)triethylammonium bromide (QX-314; Tocris Bioscience, Bristol, UK). pH was adjusted to 7.3 with KOH. Lucifer yellow was added at a concentration of 1 mg ml^{-1} to the intracellular solution for visualization of cells at the end of the recordings (whole-cell and patch). Theoretical liquid junction potentials were calculated with the computer program JPCalcW (Molecular Devices, Sunnyvale, CA, USA) and membrane holding potentials were automatically corrected online for liquid junction potentials.

Drugs were added directly to the extracellular solution used to perfuse the slices. For recordings of spIPSCs, the extracellular solution contained (μM; Tocris Bioscience): 3 bicuculline methchloride, 10 6-cyano-7-nitroquinoxaline-2,3-dione (CNQX) and 0.3 tetrodotoxin (TTX). Solutions were either made up freshly for each experiment or prepared from concentrated aliquots stored at −20°C. CNQX was first dissolved at 100 mM in dimethylsulfoxide (Sigma, St Louis, MO, USA) and then diluted to the final concentration.

Fast drug application

Ultrafast drug application was performed according to the description of Jonas (1995) and as detailed in Veruki *et al.* (2003). Drugs were applied from a theta-tube application pipette (septum thickness ∼117 μm; final tip diameter ∼300 μm; Hilgenberg, Malsfeld, Germany). The pipette tip with the outside-out patch was positioned near the interface between the control solution and

agonist-containing solution continuously flowing out of each barrel, about 100 μm away from the tip of the application pipette. Concentration jumps of agonist to the patch were performed by rapidly moving the application pipette and thus the interface between the two solutions. Drugs were dissolved in Hepes-buffered solution containing (mM): 145 NaCl, 2.5 KCl, 2.5 $CaCl_2$, 1 $MgCl_2$, 5 hemisodium-Hepes, 10 glucose, pH adjusted to 7.4 with HCl. For any concentration of glycine (May and Baker Ltd, Dagenham, UK), it replaced an equimolar concentration of NaCl. Agonist pulses were applied every 5–10 s. The solution exchange time was measured as previously described (Veruki *et al.* 2003). Under optimal conditions, the 20–80% rise time of the solution exchange ranged from 200 to 400 μs.

Electrophysiological recording and data acquisition

Voltage-clamp recordings were made with either an EPC9-dual or EPC10-triple amplifier (HEKA Elektronik, Lambrecht, Germany) controlled by either Pulse or PatchMaster software (HEKA Elektronik). Cells and patches were held at a potential of −60 mV. The signals were typically low-pass filtered with a corner frequency (−3 dB) of 5 kHz, and sampled at 50 kHz. Capacitative currents caused by the recording pipette capacitance (C_{fast}) and the cell membrane capacitance (C_{slow}) were measured with the automatic capacitance neutralization network feature of the amplifier that also estimated the series resistance (R_{series}). The average capacitance in the whole-cell recordings was 3.4 ± 0.3 pF (mean ± S.E.M.) ($n = 19$). Throughout every continuous recording of spontaneous synaptic currents, R_{series} was regularly monitored (every 60 s) by acquiring the responses to a series of 20 mV hyperpolarizing voltage pulses (16 ms duration). During such stimulation, the C_{slow} neutralization circuitry was transiently disabled. The capacitative transients were analysed off-line by averaging consecutive responses (typically 15–20) and fitting the decay with double or triple-exponential functions in order to estimate the peak capacitative current and calculate R_{series}. The average R_{series} in whole-cell recordings of cells with spIPSCs was 15.5 ± 1.6 MΩ ($n = 8$). The average holding current in whole-cell recordings was -5.6 ± 1.6 pA ($n = 19$).

General data analysis

Data were analysed with PulseFit/PulseTools, FitMaster (HEKA Elektronik), IGOR Pro (WaveMetrics, Lake Oswego, OR, USA), AxoGraph (AxoGraph Scientific, Sydney, Australia) and TAC (Bruxton Corp., Seattle, WA, USA). Spontaneous postsynaptic currents (spPSCs) were detected with a threshold of 5–7 pA depending on the noise level (MiniAnalysis; Synaptosoft, Decatur, GA, USA) and verified by eye. For amplitude and interevent interval analyses, complex PSCs, i.e. PSCs consisting of temporally overlapping events, were analysed as described by Veruki *et al.* (2003). For kinetic and non-stationary noise analyses, we included only well-separated (interevent intervals ≥ 200 ms), monophasic PSCs which appeared to rise in a monotonic fashion without visible deviation of the rising phase (cf. Traynelis *et al.* 1993) and which decayed exponentially. For kinetic analysis of averaged PSCs, the number of individual events for each cell ranged between 35 and 465. Before averaging, individual spPSCs were aligned along the point of steepest rise.

The decay time course of individual and averaged PSCs, as well as responses evoked by the ultrafast application of agonist, was estimated by curve fitting with exponential functions. For single-exponential functions we used the function:

$$I(t) = A\exp(-t/\tau) + I_{ss} \quad (1)$$

where $I(t)$ is the current as a function of time, A is the amplitude at time 0, τ is the time constant, and I_{ss} is the steady-state current amplitude (typically zero). For double-exponential functions we used the function:

$$I(t) = A_1\exp(-t/\tau_1) + A_2\exp(-t/\tau_2) + I_{ss} \quad (2)$$

where $I(t)$ is the current as a function of time, A_1 and A_2 are the amplitudes of the first and second exponential components, τ_1 and τ_2 are the time constants of the first (fast) and second (slow) exponential components and I_{ss} is the steady-state current amplitude (typically zero). Fitting was started 300–750 μs after the peak amplitude (typically 500 μs for PSCs). For double-exponential functions the amplitude contribution was calculated as $100\% \times (A_x/(A_1 + A_2))$. The weighted decay time constant was calculated as $(a_1\tau_1 + a_2\tau_2)$, where a_1 and a_2 are the relative amplitudes of the two exponential components, and τ_1 and τ_2 are the corresponding time constants. For waveforms fitted with double-exponential functions (spontaneous PSCs and evoked responses in patches), we defined time 0 as the start of the response (determined by eye as the point in time at which the current rose from the baseline noise).

In cases where step transitions corresponding to single-channel gating could be directly observed in the later portions of glycine responses, all-point amplitude histograms were constructed from selected epochs and fitted with sums of Gaussian distributions to obtain the mean current of the open level (TAC; maximum likelihood algorithm). The single-channel current was taken as the difference between the open-channel peak and the baseline. The single-channel chord conductance (γ) was calculated as:

$$\gamma = i/(E_m - E_{rev}) \quad (3)$$

from the known holding potential (E_m; −60 mV) and assuming $E_{rev} = 0$ mV.

Data are presented as means ± S.E.M. (n = number of cells, events or patches) and percentages are presented as percentage of control. Statistical analysis of correlations (either between time and a parameter for stability analysis or between two parameters) was performed using Spearman's rank order correlation test. Differences were considered significant at the $P < 0.05$ level. For illustration purposes, most raw data records were low-pass filtered (digital non-lagging Gaussian filter; −3 dB at 1–2 kHz; 500 Hz for traces with discrete single-channel transitions). Unless otherwise noted, the current traces in the figures represent individual traces.

Non-stationary noise analysis

To obtain the conductance of glycine receptor channels in outside-out patches, we applied non-stationary noise analysis (Sigworth, 1980) to responses evoked by ultra-fast applications of glycine (3 mM; 2 or 5 ms pulses; 12–189 repetitions evoked every 10 s). The sampling frequency was 50 kHz and the records were low-pass filtered at 5 kHz. For patches with no obvious rundown, the ensemble variance was calculated as the variance about each sample point in the ensemble mean. When there was evidence of rundown, the ensemble variance was calculated from the differences of overlapping pairs of successive responses as $\sigma^2 = \langle \Delta^2 \rangle / 2$, where Δ is the difference of successive records, and $\langle \Delta^2 \rangle$ is the ensemble average (expectation value) of the squared differences of successive records (Heinemann & Conti, 1992). The ensemble mean response was binned into 50 equal segments along the ordinate, such that each bin, on average, corresponded to an equal number of channel closings during the decay phase (Traynelis *et al.* 1993). The ensemble mean response and variance were averaged within each bin. Finally, the ensemble variance was plotted against the mean current (omitting the rising phase of the response) and fitted with the function:

$$\sigma^2(I) = iI - I^2/N + \sigma_b^2 \qquad (4)$$

where i is the apparent single-channel current, I is the mean current, N is the number of available channels in the patch and σ_b^2 is the variance of the background noise. The open probability (P_{open}) at any given time is determined by the equation $P_{open} = I/iN$. The single-channel conductance was calculated by eqn (3).

To obtain the conductance of synaptic glycine receptor channels, we applied peak-scaled non-stationary noise analysis (Traynelis *et al.* 1993) to ensembles of spPSCs (low-pass filtered at 5 kHz and sampled at 50 kHz). For selection of spPSCs for noise analysis, we followed the procedure described by Momiyama *et al.* (2003). Briefly, individual spPSCs were first low-pass filtered at 2 kHz (digital Gaussian filter) and analysed by measuring peak amplitude, 20–80% rise time and decay time constant. For the latter measurement, we used a single-exponential function, despite the finding (see Results) that ensemble averages were best fitted with double-exponential functions. Measured parameters were then numbered according to the event number and tested by Spearman's rank order correlation test for time stability (using a variable size, sliding window algorithm implemented in IGOR Pro, code adapted from that in the NeuroMatic package; www.physiol.ucl.ac.uk/research/silver_a/). From the complete recording of an individual cell, the algorithm returned a maximum number of consecutive spPSCs whose parameters did not display any significant correlations ($P > 0.05$). After testing for correlations between rise time and amplitude and between rise time and decay time constant (Spearman's rank order correlation test; see Results), spPSCs were used for noise analysis without the imposed digital (2 kHz) Gaussian filter. The number of events for each cell that passed these criteria and were used for noise analysis represented 70–100% of the total number of events recorded from a given cell.

To correct for quantal variability (Traynelis *et al.* 1993), the synaptic currents were analysed with peak-scaled non-stationary noise analysis. Before calculating the ensemble mean PSC, the individual spPSCs were aligned along the point of steepest rise between onset and peak. The peak of the mean current response waveform was scaled to the response value at the corresponding point in time of each individual event before subtraction to generate the difference waveforms. The ensemble mean PSC was binned (see above) and variance *versus* mean curves were plotted for the decay phase of the PSC. The curve was fitted with eqn (4) to obtain an estimate for the single-channel current (i). Depending on the shape of the variance *versus* mean curve (parabolic *versus* skewed; see Hartveit & Veruki (2006)), either the whole or a subregion (∼75%; excluding the rightmost data points) of the curve was used for curve fitting. The single-channel chord conductance was calculated from eqn (3).

Results

Identification of wide-field amacrine cells in retinal slices

This study includes results from 30 wide-field amacrine cells (19 whole-cell recordings and 11 outside-out patch recordings). The criteria used to visually target wide-field amacrine cells for recording were identical to those used to target AII amacrine cells (Gill *et al.* 2006). The targeting criteria were as follows: (1) location of the cell body at and across the border between the inner nuclear layer and the inner plexiform layer; (2) medium size of the cell body; and (3) a relatively thick primary dendrite

that tapers as it descends into the inner plexiform layer. In most cases, these criteria resulted in recordings from AII amacrine cells, but in a smaller number of cases, we recorded instead from amacrine cells that displayed the characteristic morphology of wide-field amacrine cells. During whole-cell recordings from wide-field amacrine cells, we never observed unclamped action currents similar to those characteristically seen in AII amacrine cells (5 mV depolarizing test pulses from a holding potential of −60 mV; Mørkve *et al.* (2002)). All cells were filled with Lucifer yellow and after both whole-cell and outside-out patch recordings, fluorescence microscopy allowed visualization of each cell's morphology (Fig. 1*A*). For all the wide-field cells included in this study, fluorescence microscopy revealed long, thin processes, narrowly monostratifying in a single stratum (S) of the inner plexiform layer. The cells recorded from in this study stratified in S2, S3 or S4 (see examples in Fig. 1*A*). Laterally, the processes could extend beyond the microscope's field of view or could appear truncated at some distance from the soma. We often observed small varocisities and spine-like protrusions along the length of the processes. Based on the general morphological characteristics, as observed in the vertical slice preparation, we hypothesize that these cells are the rat counterparts to some of the types of wide-field amacrine cells described in detail in rabbit and mouse retina (Famiglietti, 1992*a*,*b*; MacNeil & Masland, 1998; MacNeil *et al.* 1999; Völgyi *et al.* 2001; Badea & Nathans, 2004; Lin & Masland, 2006). On the basis of Golgi-staining, the morphology of a few types of wide-field amacrine cells has also been described in whole-mounts of rat retina (Perry & Walker, 1980); however, the level of stratification in the inner plexiform layer was not reported with sufficient precision that an identification can reliably be made for cells only observed in vertical sections, as in our study. On this background, we have not attempted to classify each cell recorded from as the rat equivalent of a particular type of wide-field amacrine cell. We were not able to determine if the wide-field amacrine cells recorded from were axon-bearing or not.

In whole-cell recordings of wide-field amacrine cells we observed spontaneous, inward PSCs (Fig. 1*B*). Under conditions where these PSCs were identified as glycinergic IPSCs (see below), their kinetic properties were strikingly different from those of glycinergic IPSCs previously observed in AII amacrine cells (Fig. 1*C*; Gill *et al.* 2006). While the IPSCs in AII amacrine cells displayed a very fast decay time course (Fig. 1*C*), the IPSCs in the wide-field amacrine cells displayed a very slow decay time course (Fig. 1*B* and *C*). Here, we demonstrate that the slow decay time course of IPSCs in wide-field amacrine cells is a direct consequence of the kinetic properties of the glycine receptors expressed by these cells.

Spontaneous PSCs in wide-field amacrine cells

To isolate the action of glycine receptors on wide-field amacrine cells, whole-cell recordings were carried out in the presence of CNQX, TTX and bicuculline in order to block non-NMDA receptors, voltage-gated Na^+ channels and $GABA_A$ receptors, respectively. Bicuculline was used at a concentration of 3 μM that presumably does not block glycine receptors (Protti *et al.* 1997; Jonas *et al.* 1998; Wang & Slaughter, 2005; Gill *et al.* 2006). Of the 19 wide-field amacrine cells that we made whole-cell recordings from, eight cells displayed spPSCs in this condition. All of these cells had processes stratifying in S2 of the inner plexiform layer. The spPSCs occurred at a low, irregular frequency (1.4 ± 0.3 Hz, range 0.29–2.3 Hz, $n = 8$). Seven of these cells had enough spPSCs to contruct histograms of interevent intervals, which were well fitted by single-exponential functions (average time constant $\tau = 0.50 \pm 0.08$ s), suggesting individual events occurred independently (Fig. 1*D*). Amplitude histograms were skewed towards larger values. For the example shown in Fig. 1*E*, the mode was ∼12.5 pA and the mean was 21.5 ± 1.1 pA (range 5–142 pA). The coefficient of variation was 0.79 for this cell. For the eight wide-field amacrine cells (range 50–921 events), the mode occurred at 14.5 ± 2.3 pA (range 7–31 pA) and the mean was 23 ± 5 pA (range 12–55 pA). The coefficient of variation varied between 0.28 and 1.0 (average 0.63 ± 0.09).

In AII amacrine cells, 300 nM of the specific glycine receptor antagonist strychnine is sufficient to block both spIPSCs and responses evoked by application of glycine to outside-out patches (Gill *et al.* 2006). In wide-field amacrine cells, spPSCs were completely and reversibly blocked by 300 nM strychnine (Fig. 1*F*; $n = 4$). The small, inwardly directed noise transients remaining in the presence of strychnine (Fig. 1*F*) could not be reliably identified as spIPSCs because the amplitude was too low, but could suggest that 3 μM bicuculline is not sufficient to completely block $GABA_A$ receptors in wide-field amacrine cells (cf. Protti *et al.* 1997). Based on this evidence, we consider the spPSCs recorded in the conditions described here to be glycinergic IPSCs. The low incidence of recording of wide-field amacrine cells precluded a more detailed pharmacological analysis.

Time course of spontaneous glycinergic IPSCs in wide-field amacrine cells

To examine the kinetic properties of the glycinergic spIPSCs, we selected well-separated events with monophasic waveforms. For five wide-field amacrine cells, each with more than 100 spIPSCs, we measured kinetic parameters for individual events and for ensemble averages. For the representative example illustrated in

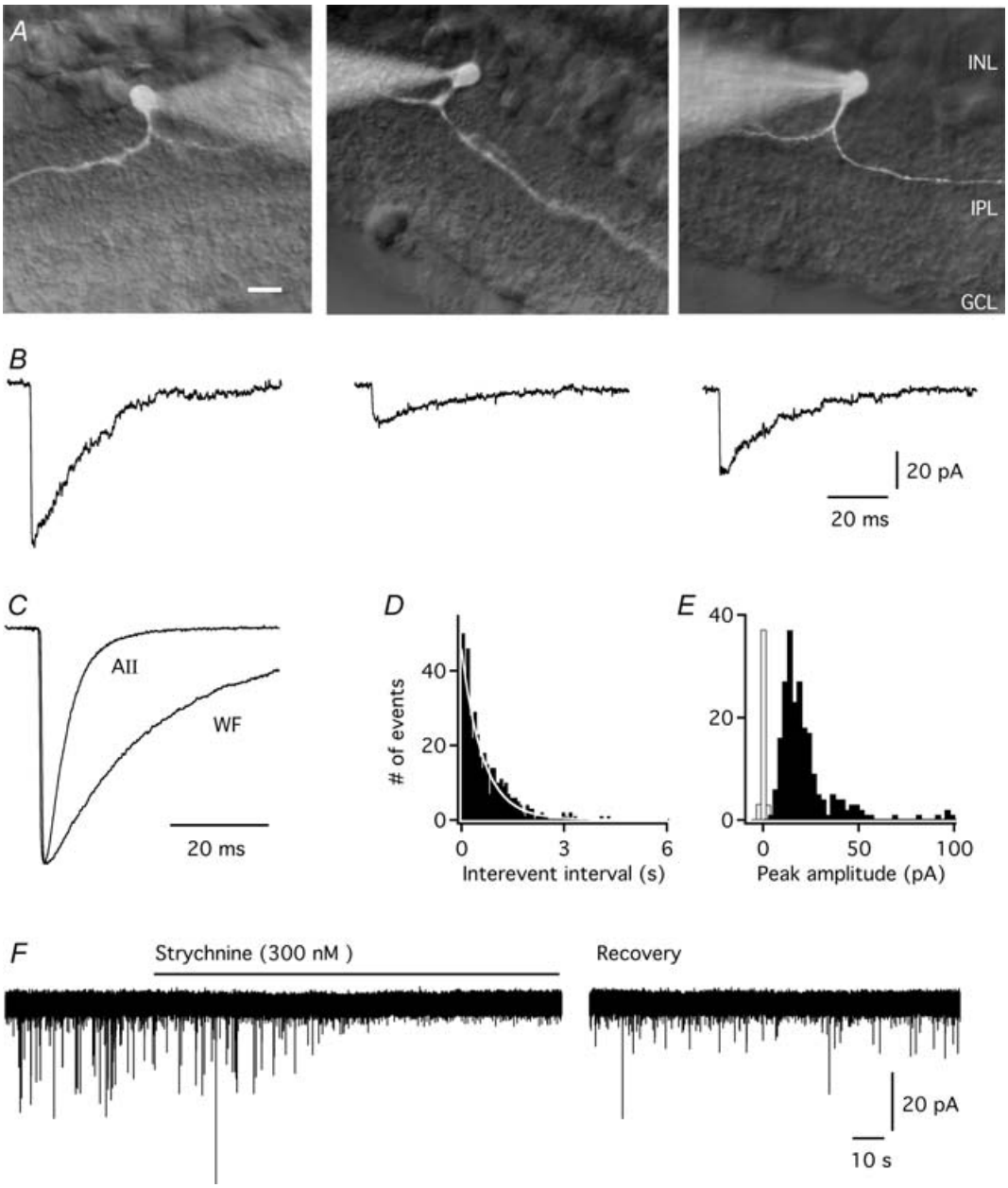

Figure 1. Properties of glycinergic spontaneous inhibitory postsynaptic currents (spIPSCs) in wide-field amacrine cells in the rat retinal slice preparation
A, three examples of wide-field amacrine cells in an *in vitro* slice preparation from rat retina. Each cell is shown as a composite fluorescence photomicrograph (after filling with Lucifer yellow) overlaid on a retinal slice visualized with infrared differential interference contrast videomicroscopy. Each cell has long thin processes that narrowly stratify in a single stratum of the inner plexiform layer (left: S2; middle: S2; right: S3). Retinal layers are indicated by abbreviations (right: INL, inner nuclear layer; IPL, inner plexiform layer; GCL, ganglion cell layer). Scale bar, 10 μm. *B*, three examples of slowly decaying spIPSCs recorded in a wide-field amacrine cell. Data from the same cell in *B–E*. *C*, average waveform of spIPSCs ($n = 242$ events) in the wide field amacrine cell (WF). For comparison, the waveform has been plotted with an average waveform of spIPSCs ($n = 166$ events) recorded in an AII amacrine cell (data from Fig. 1*C* in Gill *et al.* 2006). Notice the much slower decay time course in the wide-field compared to the AII amacrine cell. The averaged waveforms were aligned at onset after normalization of peak amplitudes. *D*, interevent interval histogram of spIPSCs; single-exponential fit indicated by white line; bin width 70 ms. *E*, amplitude distribution of spIPSCs; notice the skew towards larger amplitudes; bin width 2.5 pA. One event with a peak amplitude of 142 pA is not shown. The noise distribution is shown as an unfilled histogram (peak scaled to the peak of the IPSC amplitude distribution). *F*, bath application of 300 nM strychnine rapidly blocks spIPSCs in a wide-field amacrine cell (because of the slow time scale, spIPSCs appear as downward spikes). The spIPSCs recovered slowly during washout of strychnine.

Fig. 2, the peak amplitude of individual spIPSCs varied from 6 to 70 pA (Fig. 2*A*; average 32.6 ± 0.7 pA). The 20–80% rise time of the individual spIPSCs varied from 150 to 910 μs (Fig. 2*B*; average 326 ± 7 μs). The decay phase of individual spIPSCs was moderately well fitted by single-exponential functions (Fig. 2*D*) with τ_{decay} varying from 10 to 139 ms (Fig. 2*C*; average 42 ± 1 ms). For analysis of the average spIPSC, the decay phase was better fitted with a double-exponential function (Fig. 2*E*; $\tau_{fast} = 19$ ms, $\tau_{slow} = 85$ ms; amplitude contribution 66% and 34%, respectively) than with a single-exponential function (not shown; $\tau_{decay} = 37$ ms).

For this and the other four cells with more than 100 spIPSCs, there was no correlation between 20–80% rise time and τ_{decay} (Fig. 2*F*), suggesting the absence of differential electrotonic filtering. Furthermore, for this and another cell there was no correlation between 20%–80% rise time and peak amplitude (Fig. 2*G*), but for three of the five cells, there was a significant negative correlation between these parameters, suggesting the presence of differential electrotonic filtering (Spearman's rank order correlation test; Spearman's R varied between -0.54 and -0.30; $P < 0.0001$). Although it is very likely that spIPSCs originating at distal locations in

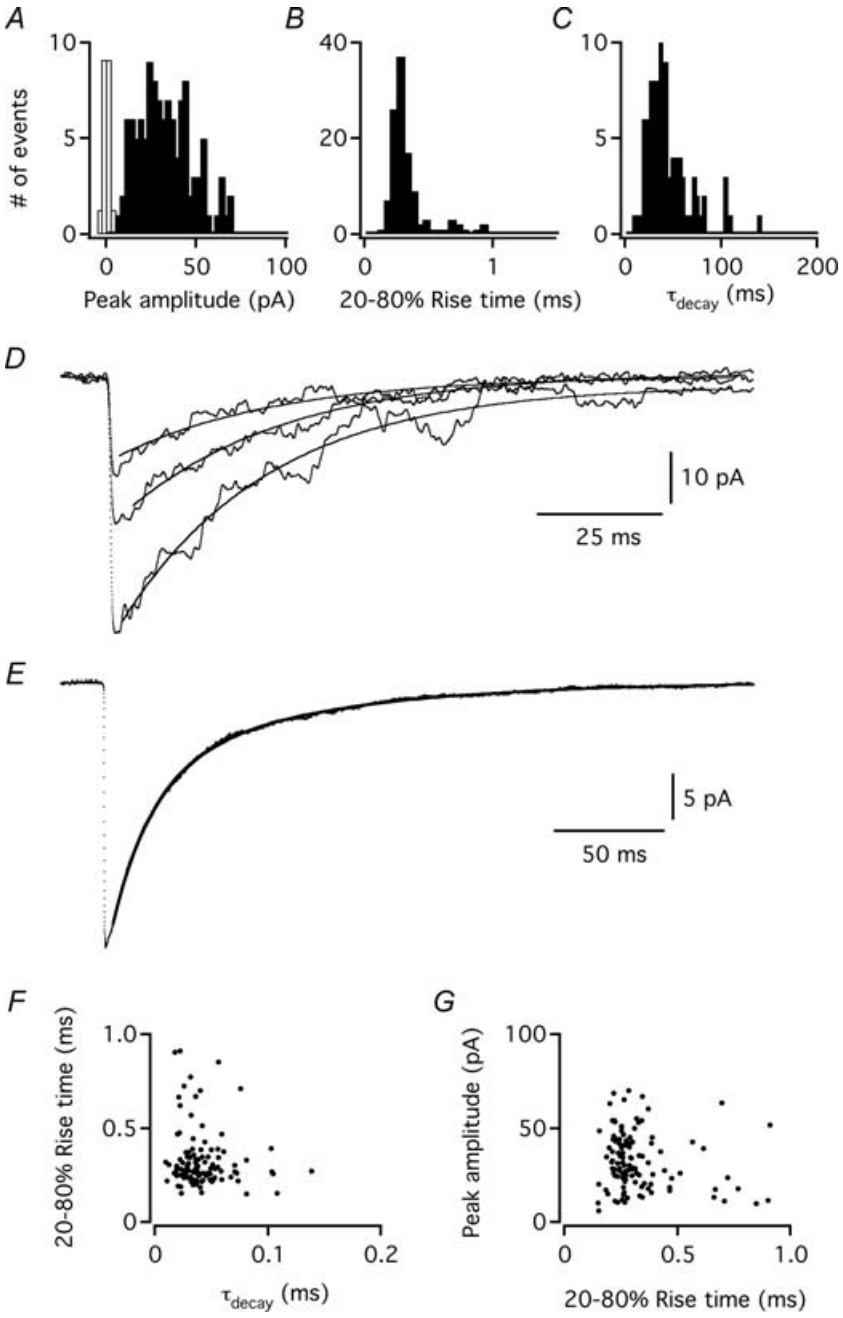

Figure 2. Kinetics of glycinergic spIPSCs in wide-field amacrine cells
A, amplitude distribution of spIPSCs in a wide-field amacrine cell ($n = 114$ events); bin width 2.5 pA. The noise distribution is shown as an unfilled histogram (peak scaled to the peak of the IPSC amplitude distribution). Data from the same cell in *A*–*G*. *B*, distribution of 20–80% rise time for spIPSCs; bin width 0.05 ms. *C*, distribution of τ_{decay} (single-exponential fit) for spIPSCs; bin width 2.5 ms. *D*, three overlaid spIPSCs (dotted lines), aligned by the point of steepest rise. A single-exponential fit (continuous line) has been overlaid on decay phase of each spIPSC. *E*, average waveform of spIPSCs (dotted line) overlaid with a double-exponential fit (continuous line). *F*, relation between spIPSC 20–80% rise time and τ_{decay}. *G*, relation between spIPSC peak amplitude and 20–80% rise time.

the dendritic tree of a wide-field amacrine cell would be subject to marked electrotonic filtering, the lack of correlation between 20%–80% rise time and τ_{decay} suggests that the range of observed values for τ_{decay} cannot solely be explained by differential electrotonic filtering of identical, fast events originating at different locations in the dendritic tree. It is also likely that a substantial fraction of the recorded spIPSCs originated from relatively proximal regions of the dendritic tree of the wide-field amacrine cells, either because of a corresponding spatial restriction in the location of glycinergic synaptic input, or, alternatively, because of truncation of cellular processes during the slicing procedure and a corresponding removal of distant synaptic input. A proximal origin for many spIPSCs is supported by the relatively fast rise times of the majority of spIPSCs.

Kinetic properties of ensemble averages were measured for all eight wide-field amacrine cells that displayed glycinergic spIPSCs, with the number of events ranging between 35 and 465. The population average of the 20–80% rise time was $340 \pm 53\ \mu$s (range 250–630 μs). For comparison with other published reports, the average 10–90% rise time was $570 \pm 110\ \mu$s (range 390–1200 μs). For each cell, the decay phase of the average spIPSC was best fitted by a double-exponential function ($\tau_{fast} = 15 \pm 2$ ms; $77 \pm 2\%$ amplitude contribution; $\tau_{slow} = 57 \pm 7$ ms; $23 \pm 2\%$ amplitude contribution). The amplitude-weighted τ_{decay} was 25 ± 3 ms. When the decay phase was fitted with a single-exponential function, the average τ_{decay} was 26 ± 4 ms (not shown).

Non-stationary noise analysis of glycinergic spIPSCs in wide-field amacrine cells

For the five wide-field amacrine cells with more than 100 events (see above), we tested for time stability by systematically searching the recording for a consecutive series of spIPSCs with no time-dependent change in either peak amplitude, 20–80% rise time or τ_{decay} (Fig. 3*A*–*C*; cf. Momiyama *et al.* 2003). For each of the five cells, such regions were identified, with Spearman's R varying between -0.13 and 0.10 for peak amplitude, between -0.01 and 0.13 for 20–80% rise time and between -0.03 and 0.18 for τ_{decay} ($P = 0.25 \pm 0.10$ for peak amplitude; $P = 0.61 \pm 0.14$ for 20–80% rise time; $P = 0.42 \pm 0.16$ for τ_{decay}).

Because of quantal variability, with the number of available receptor channels varying from one spIPSC to the next, we employed peak-scaled non-stationary noise analysis (Traynelis *et al.* 1993) and scaled the peak of the ensemble mean waveform (Fig. 3*F*) to each individual spIPSC (Fig. 3*D*) before we calculated the difference currents (Fig. 3*E*) and the ensemble variance (Fig. 3*G*). For the cell illustrated in Fig. 3, peak-scaling resulted in a moderately skewed (as opposed to parabolic) variance *versus* mean curve (Fig. 3*H*; see Hartveit & Veruki (2006)). Curve fitting with eqn (4) ($\sim$60% of the curve), gave a unitary current (i) of 2.2 pA, corresponding to a unitary chord conductance (γ) of 37.1 pS. For the five cells, peak-scaled non-stationary noise analysis gave a unitary chord conductance of 34 ± 4 pS (range 24–48 pS).

Deactivation and desensitization kinetics of glycine receptors in outside-out patches from wide-field amacrine cells

The analysis of spIPSCs in wide-field amacrine cells demonstrated markedly slow decay kinetics compared to spIPSCs in AII amacrine cells (Gill *et al.* 2006). The slow decay could be due to the expression of synaptic glycine receptor channels with slow kinetic properties. Alternatively, the slow decay could be due to slow clearance of transmitter from the synaptic cleft. A third possibility is that the slow decay is related to the neuronal morphology with long, thin processes, giving rise to inadequate space-clamp and pronounced electrotonic filtering. In order to directly investigate the kinetic properties of glycine receptor channels in wide-field amacrine cells, we measured responses evoked by ultrafast application of glycine to somatic outside-out patches. Figure 4*A* illustrates the response evoked by a short ($\sim$5 ms) pulse of glycine (3 mM) to a patch from a wide-field amacrine cell. The response rose rapidly to a peak with a 20–80% rise time of 360 μs. For nine patches, the 20–80% rise time of responses evoked by brief (2–5 ms) pulses was $610 \pm 79\ \mu$s (range 360–1020 μs). At the end of the pulse, the response decayed very slowly. This deactivation, which reflects the closure of channels after removal of agonist, was well fitted by a double-exponential function. For the patch shown in Fig. 4*A*, τ_{fast} was 74 ms and τ_{slow} was 410 ms. The amplitude contributions were 66% and 34%, respectively. The average τ_{fast} was 45 ± 5 ms ($64 \pm 7\%$ amplitude contribution) and the average τ_{slow} was 350 ± 56 ms ($36 \pm 7\%$ amplitude contribution; $n = 9$). For the patch illustrated in Fig. 4*A*, the amplitude weighted τ_{decay} was 190 ms (average $= 170 \pm 39$ ms). When the time course of deactivation was fitted with a single-exponential function, we obtained a τ_{decay} of 190 ms (average 160 ± 47 ms). The deactivation kinetics of patches from wide-field amacrine cells were considerably slower than the deactivation kinetics previously observed for patches from AII amacrine cells (Gill *et al.* 2006; Fig. 4*B*).

For some patches from wide-field amacrine cells, we also applied longer pulses of glycine (3 mM) in order to study desensitization. The time course of desensitization, reflecting the closure of channels in the maintained presence of glycine, was even slower than the time course of deactivation. For the wide-field

amacrine cell responses illustrated in Fig. 4*C*, the decay could be well fitted with a double-exponential function with $\tau_{fast} = 24$ ms and $\tau_{slow} = 670$ ms. The amplitude contributions were 35% and 65%, respectively. For a total of eight patches, the average τ_{fast} was 43 ± 10 ms (53 ± 8% amplitude contribution) and the average τ_{slow} was 680 ± 170 ms (47 ± 8% amplitude contribution). The average amplitude-weighted τ_{decay} was 380 ± 150 ms. The equilibrium response to 3 mM glycine was measured as the current at the end of the 1000 ms application, and was on average 32 ± 3% of the peak response.

While glycinergic spIPSCs were only observed in wide-field amacrine cells stratifying within S2, glycine-evoked responses in outside-out patches were obtained in all types of wide-field amacrine cells recorded from, including those with processes stratifying in S2, S3 and S4. Although our material is too small for statistical testing of potential differences in response

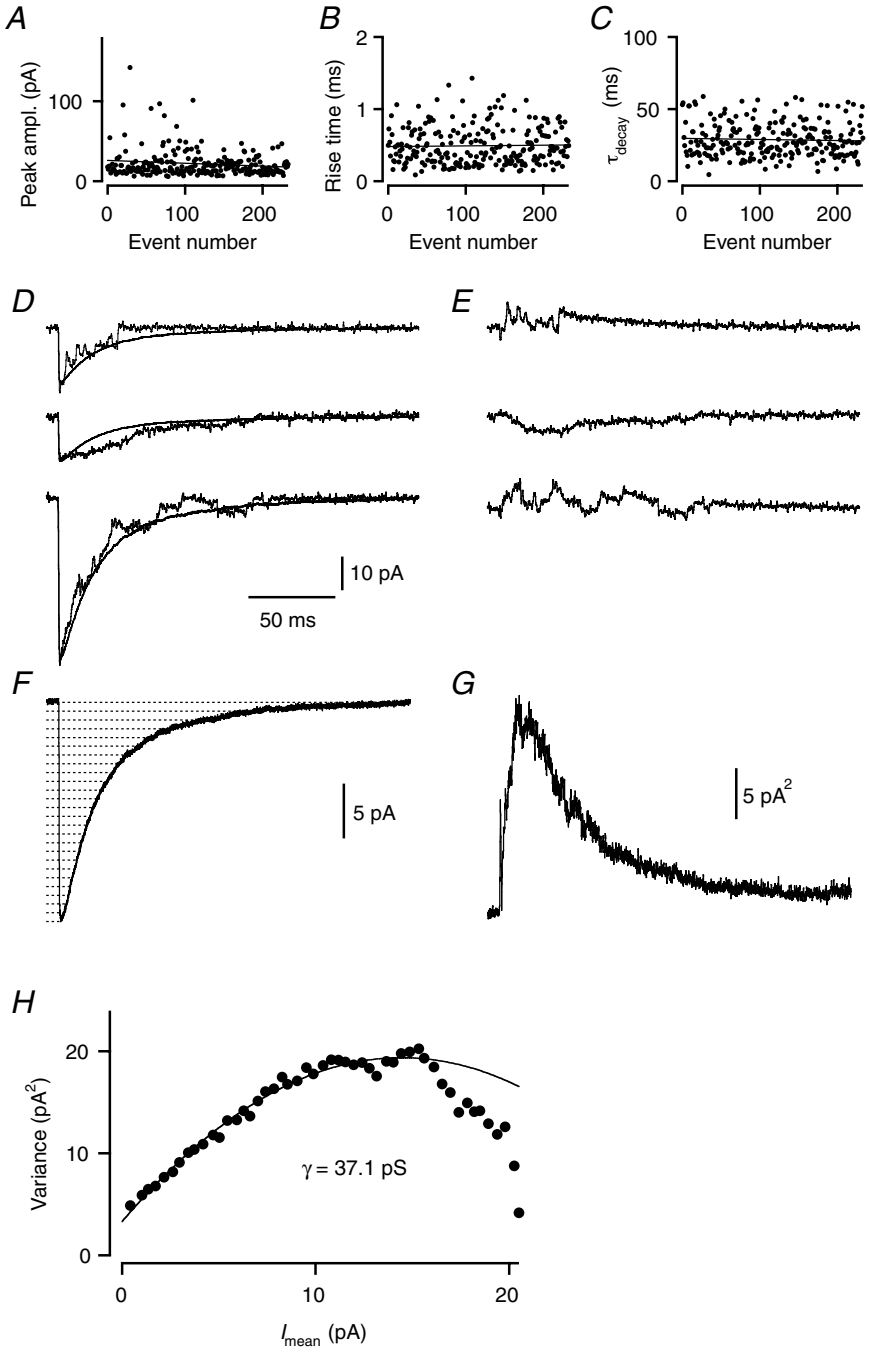

Figure 3. Non-stationary noise analysis of glycinergic spIPSCs in a wide-field amacrine cell
A–C, plots of peak amplitude (*A*), 20–80% rise time (*B*) and τ_{decay} (*C*) for 244 consecutive spIPSCs; no time-dependent correlation (linear fit in each graph). *D*, three individual spIPSCs from the population in *A–C*, superimposed mean spIPSC (smooth curves) after peak-scaling waveform to each individual spIPSC (see Methods). Same time scale in *D–G*. *E*, three difference currents calculated from corresponding individual spIPSCs and peak-scaled mean spIPSC in *D*. Amplitude scale as in *D*. *F*, ensemble mean spIPSC. Dotted horizontal lines indicate amplitude intervals used for binning mean current and variance (see Methods), for clarity only every other bin is shown. *G*, ensemble current variance (without binning) for the spIPSCs, calculated from the difference traces between individual spIPSCs and the peak-scaled mean spIPSC (as in *E*). *H*, plot of ensemble current variance calculated with peak-scaling (*G*) *versus* mean current (*F*; after binning). Time range used for the variance *versus* mean plot corresponds to data points from the peak of the mean spIPSC to the end of the decay phase. The data points were fitted with eqn (4).

kinetics between cells stratifying at different levels of the inner plexiform layer, the data did not suggest the presence of such differences.

Non-stationary noise analysis of transient currents evoked by glycine in outside-out patches from wide-field amacrine cells

When spIPSCs were analysed by non-stationary noise analysis, peak-scaling precluded any measurement of P_{open}. In order to estimate the single-channel current and maximum P_{open} of glycine receptors in wide-field amacrine cells, we used non-stationary noise analysis of responses evoked by ultrafast application of brief pulses of 3 mM glycine to outside-out patches from wide-field amacrine cells. Figure 5*A* shows three individual, successive records evoked by glycine, and the ensemble mean is shown in Fig. 5*C*. Because of moderate rundown of the response, we estimated the ensemble variance by calculating the differences of overlapping pairs of successive responses (see Methods). Two such pairwise difference traces (for the responses in Fig. 5*A*) are shown in Fig. 5*B*, and the resulting ensemble variance is shown in Fig. 5*D*. The variance *versus* mean plot of the data points corresponding to the decaying phase is shown in Fig. 5*E* and has a clear parabolic shape, indicating that the maximum P_{open} reached a value larger than 0.5. When the data points were fitted with eqn (4), the apparent glycine-activated single-channel current was 2.0 pA, corresponding to an apparent single-channel chord conductance of 33.4 pS. The number of active channels was estimated as 28.8, corresponding to a maximum P_{open} at the peak response of 0.72 (Fig. 5*E*). For eight patches tested with glycine (3 mM), the mean single-channel chord conductance was 31 ± 3 pS (range 19–39 pS), and the mean number of available channels was 34 ± 4 (range 19–48). The average maximum P_{open} was 0.76 ± 0.03 (range 0.63–0.85).

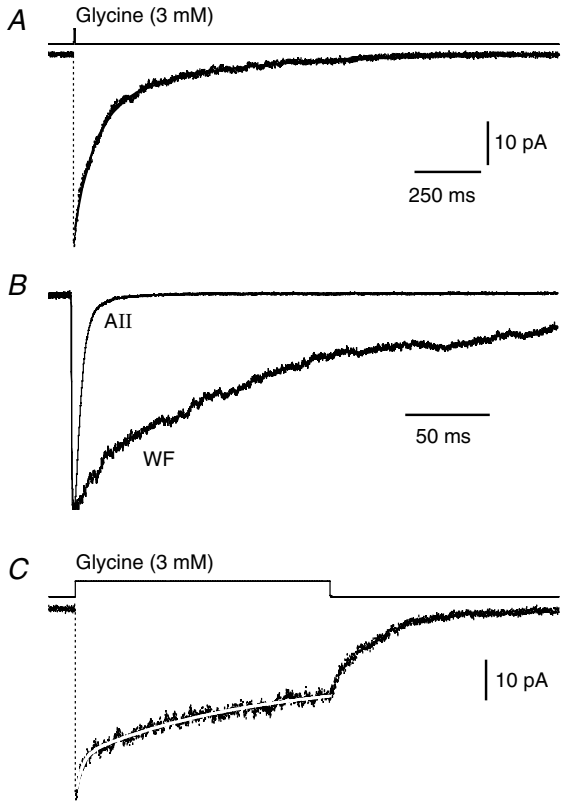

Figure 4. Deactivation and desensitization kinetics of glycine receptors in outside-out patches from wide-field amacrine cells
A, response (lower trace; dotted line; average of 25 trials) of outside-out patch to brief (∼5 ms), ultrafast application of glycine (3 mM), overlaid with a double-exponential fit to the decay phase (continuous line). Notice the very slow deactivation time course. Here and below, the upper trace illustrates the exchange time course (measured as a change in liquid junction current with an open tip pipette after breaking the patch; see Methods). *B*, for comparison of deactivation kinetics in outside-out patches from wide-field amacrine cells with deactivation kinetics in outside-out patches from AII amacrine cells, the response in *A* (wide field amacrine cell; WF) has been plotted with a corresponding response obtained from an AII amacrine cell (data from Fig. 5*A* in Gill *et al.* 2006). Notice the much slower decay time course in the wide-field compared to the AII amacrine outside-out patch. The averaged waveforms were aligned at onset after normalization of peak amplitudes. *C*, response (lower trace; dotted line, average of 16 trials) of outside-out patch (same as in *A* and *B*) to long (1 s), ultrafast application of glycine (3 mM), overlaid with a double-exponential fit to the decay phase (white continuous line). Time scale as in *A*.

Direct observations of single-channel gating in patch responses and spIPSCs

The estimates from non-stationary noise analysis potentially represent weighted averages of different conductance levels, irrespective of whether they correspond to different channels or different (sub)conductance levels of the same channels. Cull-Candy *et al.* (1988) demonstrated that the weights are determined by the relative number of channels, the single-channel conductance(s) for each channel type and their open probability. It is therefore important to investigate the relation between the apparent single-channel conductance values estimated by non-stationary noise analysis (spIPSCs or outside-out patches) and directly observed single-channel conductance levels. For several outside-out patches with low noise levels, discrete transitions between open and closed states of varying levels were apparent during later phases of individual current responses. Figure 6*A* shows the response of an outside-out patch from a wide-field amacrine cell to a brief pulse of glycine (3 mM) with several discrete transitions between open and closed states. We estimated the single-channel conductance by constructing an all-point amplitude histogram (Fig. 6*A*; inset) from a selected segment in a late phase of the response (Fig. 6*A*; legend). For the analysed segment, the single-channel current was ∼2.8 pA, corresponding to a single-channel

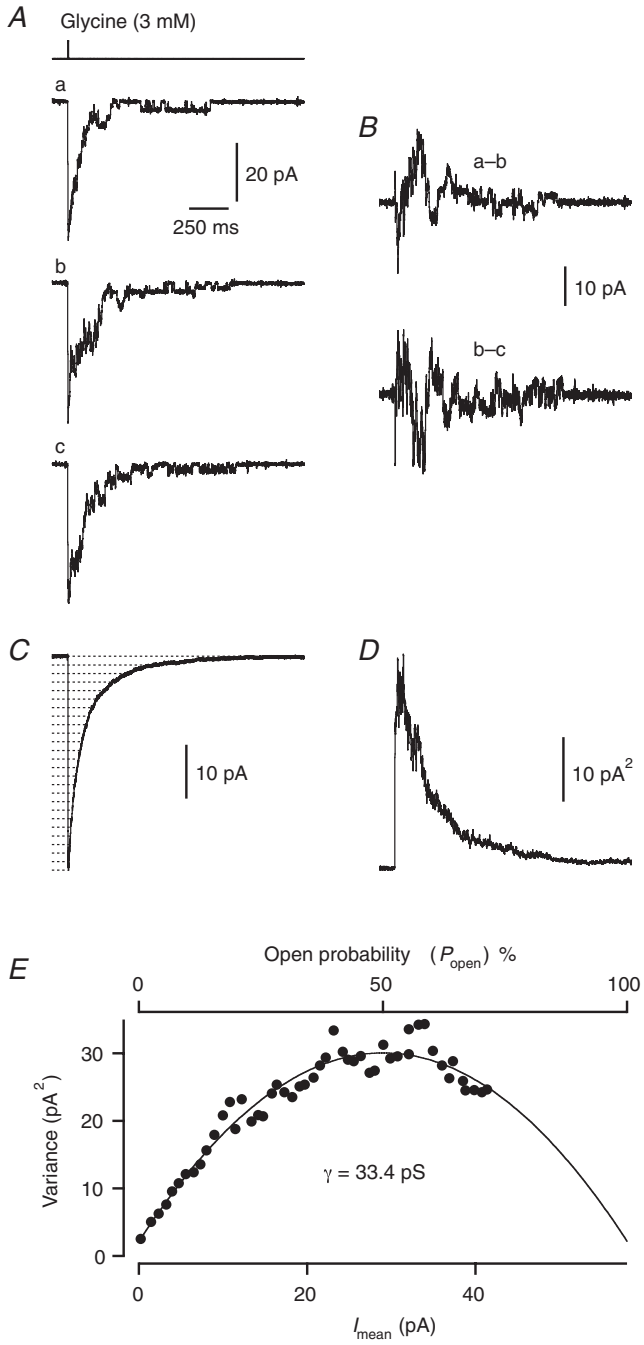

Figure 5. Non-stationary noise analysis of glycine-evoked responses in an outside-out patch from a wide-field amacrine cell

A, three individual records (a–c) obtained by brief (∼5 ms) pulses of glycine (3 mM). The upper trace illustrates the exchange time course. Same time scale in *A*–*D*. *B*, two pairwise difference currents calculated from successive individual records in *A*, upper and lower trace correspond to difference between trace 'a' and trace 'b', and between trace 'b' and trace 'c', respectively. *C*, the mean current of all glycine-evoked responses in the ensemble ($n = 189$). Dotted horizontal lines indicate amplitude intervals used for binning mean current and variance (see Methods), for clarity only every other bin is shown. *D*, ensemble current variance (without binning) for the glycine-evoked responses, calculated from the ensemble of pairwise difference currents (differences of overlapping pairs of successive responses; as in *B*). *E*, plot of ensemble current variance (*D*) *versus* mean current (*C*; after binning) and *versus* open probability. The time range used for the variance *versus* mean plot corresponds to data points from the peak of the mean waveform to the end of the decay phase. The data points were fitted with eqn (4).

chord conductance of ∼47 pS. Observations of similar single-channel openings (42–52 pS) were made for 11/11 patches. In addition, however, in several patches we also observed lower and higher current levels, corresponding to conductance levels of approximately 25–28 pS, 32–38 pS and 70–83 pS. Figure 6*B* shows a response with a segment containing repeated single-channel openings of ∼1.9 pA, corresponding to a single-channel chord conductance of ∼32 pS. Single-channel transitions with even lower amplitude were observed, but not analysed further. We never observed single-channel transitions with conductance levels around 100–110 pS, the reported main conductance level of $\alpha 2$ homomeric receptors (Bormann *et al.* 1993).

In whole-cell recordings from wide-field amacrine cells, we often observed transitions in the decay phase of spIPSCs with an amplitude of ∼2.8 pA (∼47 pS), as well as a lower amplitude of ∼2.1 pA (∼35 pS), as illustrated by the examples in Fig. 6*C*. In glycinergic spIPSCs of AII amacrine cells, we observed single-channel transitions with an amplitude of ∼5 pA (Gill *et al.* 2006), corresponding to the reported main conductance state of homomeric $\alpha 1$ receptors (∼83 pS; Bormann *et al.* 1993). We never observed transitions corresponding to this, or higher conductance levels, in spIPSCs in wide-field amacrine cells.

Discussion

In this study we have recorded glycine responses from wide-field amacrine cells in the mature, mammalian retina. All wide-field amacrine cells displayed narrowly monostratifying processes, with each type stratifying at a distinct level of the inner plexiform layer (S2, S3 or S4). The most important result is that both synaptic currents (measured as spIPSCs) and currents evoked by ultrafast application of brief pulses of glycine to outside-out patches display very slow decay kinetics, in marked contrast to the fast decay kinetics previously observed for glycine receptor currents in AII amacrine cells (Gill *et al.* 2006; see Table 1 for a detailed comparison between wide-field and AII amacrine cells). With respect to desensitization kinetics, there were no marked differences between the results for wide-field and AII amacrine cells (Table 1). The difference in decay kinetics between wide-field and AII amacrine cells suggests that unique glycine receptor properties may differentially shape glycinergic input to

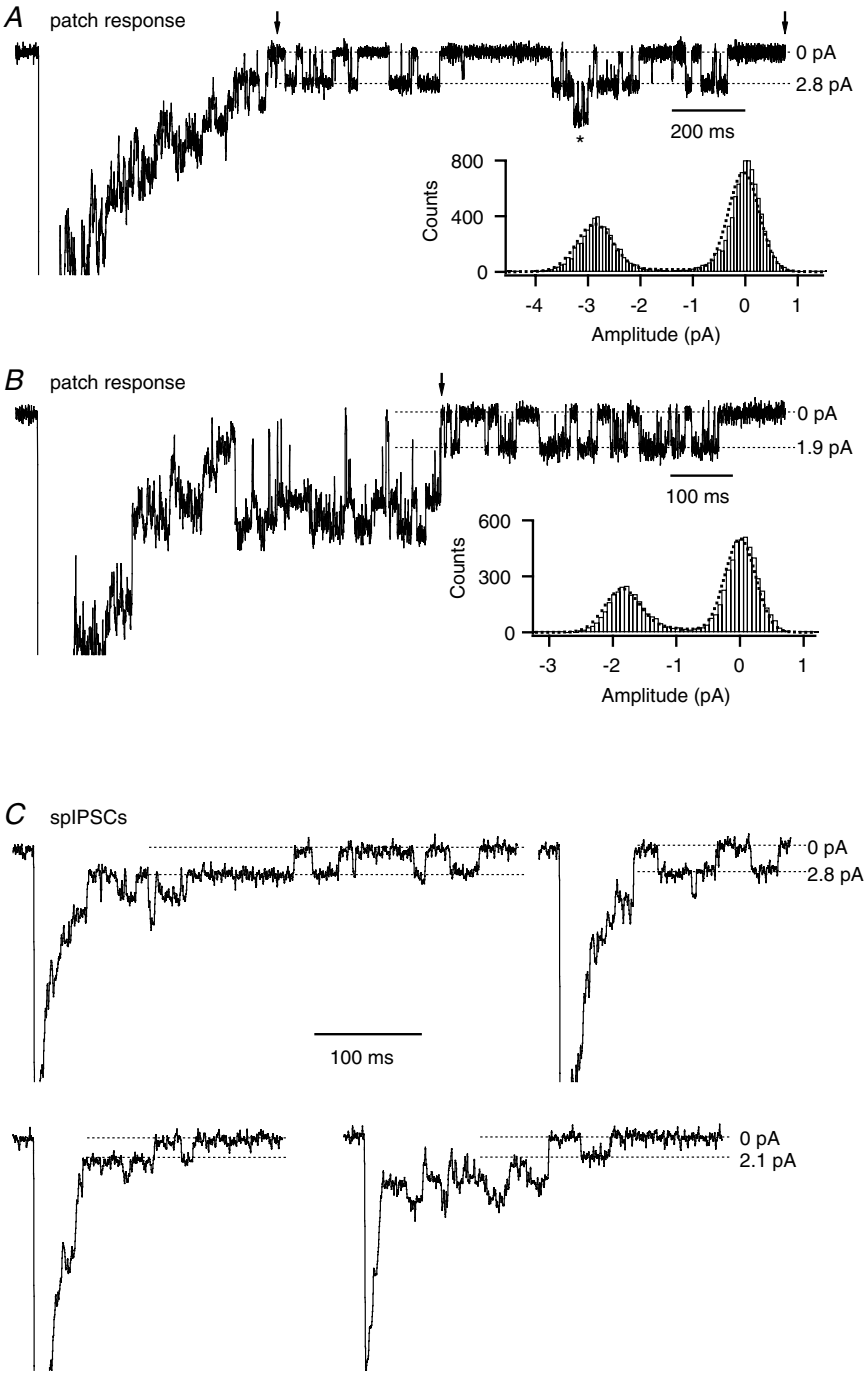

Figure 6. Single-channel conductance of glycine receptor channels in patches and spIPSCs in wide-field amacrine cells

A and *B*, current responses evoked by brief (5 ms) pulses of glycine (3 mM) to outside-out patches from wide-field amacrine cells. Here, and in *C*, the peak of response has been truncated for clarity. Notice directly resolvable single-channel gating in response to application of glycine. Here, and in *C*, dotted lines indicate either baseline current (0 pA; leak current has been subtracted) or inward current during channel opening (as indicated). Inset in *A* shows all-point amplitude histogram (bin width 0.0625 pA) for data points between two vertical arrows (excluding region marked by *). Inset in *B* shows all-point amplitude histogram (bin width 0.0625 pA) for data points between the vertical arrow and ~400 ms of additional baseline to the right of the displayed trace. Each histogram has been fitted with the sum of three Gaussian distributions (dotted line; the third distribution added to compensate for incompletely resolved transitions) and the interval between the two major peaks was taken as the single-channel current amplitude (*A* ~2.8 pA; *B* ~1.9 pA). *C*, four individual spIPSCs from wide-field amacrine cells. Notice directly resolvable single-channel gating during the decay phase of the spIPSCs (top spIPSCs ~ 2.8 pA; bottom spIPSCs ~ 2.1 pA).

Table 1. Comparison of glycine receptor data (spIPSCs and outside-out patches) for wide-field and AII amacrine cells in rat retina

	WF	AII
spIPSCs (n = number of cells)		
Rise time (μs) (20–80%)	340 ± 53 (8)	320 ± 10 (21)
τ_{fast} (ms)	15 ± 2 (8)	4.8 ± 0.2 (18)
Amplitude τ_{fast} (%)	77 ± 2 (8)	97 ± 1 (18)
τ_{slow} (ms)	57 ± 7 (8)	33 ± 5 (18)
Amplitude τ_{slow} (%)	23 ± 2 (8)	3 ± 1 (18)
Amplitude (pA)	23 ± 5 (8)	23 ± 2 (11)
CV	0.63 ± 0.09 (8)	0.61 ± 0.03 (11)
Frequency (Hz)	1.4 ± 0.3 (8)	0.45 ± 0.05 (55)
Outside-out patches (n = number of patches)		
Rise time (μs) (20–80%)	610 ± 79 (9)	700 ± 65 (8)
$\tau_{deactivation,fast}$ (ms)	45 ± 5 (9)	4.6 ± 0.5 (8)
Amplitude $\tau_{deactivation,fast}$ (%)	64 ± 7 (9)	85 ± 5 (8)
$\tau_{deactivation,slow}$ (ms)	350 ± 56 (9)	17 ± 2 (8)
Amplitude $\tau_{deactivation,slow}$ (%)	36 ± 7 (9)	15 ± 5 (8)
$\tau_{desensitization,fast}$ (ms)	43 ± 10 (8)	40 ± 15 (6)
Amplitude $\tau_{desensitization,fast}$ (%)	53 ± 8 (8)	30 ± 3 (6)
$\tau_{desensitization,slow}$ (ms)	680 ± 170 (8)	880 ± 310 (6)
Amplitude $\tau_{desensitization,slow}$ (%)	47 ± 8 (8)	70 ± 3 (6)
Equilibrium response (%)	32 ± 3 (8)	49 ± 2 (6)

Data for spontaneous inhibitory postsynaptic currents (spIPSCs) and outside-out patch responses from wide-field (WF) and AII amacrine cells. Data for outside-out patches obtained with ultrafast application of glycine (3 mM), brief pulses (2–5 ms) for measurement of deactivation kinetics and longer pulses (1 s) for measurement of desensitization kinetics. The equilibrium response was measured as the current at the end of the 1 s application relative to the peak response to the same stimulus. Data for AII amacrine cells from Gill *et al.* (2006). CV indicates coefficient of variation for peak amplitude. Values are stated as mean ± S.E.M.

different types of amacrine cells. With respect to shaping evoked synaptic responses in these and other retinal cells, the time course of presynaptic release is also likely to be an important mechanism. This underscores the importance of determining the identity and functional properties of the presynaptic sources of glycinergic input to these and other types of amacrine cells.

The present results suggest that the slow decay of spIPSCs in the wide-field amacrine cells is a direct consequence of the functional properties of the synaptic glycine receptor channels. Importantly, the results were obtained from retinas of mature animals, ruling out the possibility that slow spIPSCs in wide-field amacrine cells are specific to an early developmental stage. The specific kinetic properties of synaptic glycine receptors in wide-field amacrine cells are likely to be important for shaping the postsynaptic events during glycinergic inhibitory activity. In the context of differential expression of neurotransmitter receptors during development, it has been suggested that faster decay of postsynaptic currents might contribute to increased precision of sensory perception (Takahashi, 2005). The present results, combined with the results previously obtained for AII amacrine cells (Gill *et al.* 2006), strongly suggest that glycinergic synaptic currents with both fast and slow kinetics play important roles in sensory processing at early stages of the mature visual system. The results also suggest that there might be a larger range of functional properties of glycine receptors expressed by amacrine cells, compared to the range observed for other retinal cell types such as bipolar cells (Cui *et al.* 2003; Ivanova *et al.* 2006) and ganglion cells (Protti *et al.* 1997; Tian *et al.* 1998). This might be related to a correspondingly larger range of morphological variability among amacrine cells than among the other cell types.

The decay time course of spIPSCs in wide-field amacrine cells was best fitted by double-exponential functions, with $\tau_{fast} \sim 15$ ms and $\tau_{slow} \sim 57$ ms. A double-exponential decay has also been found in other glycinergic synapses (Legendre, 1998; Singer *et al.* 1998; Singer & Berger, 1999; Gill *et al.* 2006). The amplitude contribution of the fast component was ∼77%. Because of the special cellular morphology of wide-field amacrine cells, with long, thin processes, it is relevant to consider whether the slow decay kinetics of spIPSCs could be caused by inadequate voltage-clamp control in the dendritic tree. In this case, the slow decay kinetics would simply correspond to pronounced electrotonic filtering. While

synaptic currents originating from distant sites of the dendritic tree of wide-field amacrine cells undoubtedly would undergo a considerable degree of electrotonic filtering when the cells are voltage clamped at the soma, other observations suggest instead that the glycine receptor channels of wide-field amacrine cells have genuinely slow decay kinetics. First, although the spIPSCs in wide-field amacrine cells displayed a range of rise times, long decay times were also observed for the spIPSCs displaying the fastest rise times ($<500\ \mu s$). Second, directly resolved single-channel gating activity could be observed in spIPSCs with long decay times, suggesting that these events originated relatively close to the soma, with little electrotonic filtering. Finally, responses evoked by ultrafast application of brief pulses of glycine to outside-out patches displayed very slow deactivation kinetics. The decay phase could be well fitted by double-exponential functions, with $\tau_{fast} \sim 45$ ms and $\tau_{slow} \sim 350$ ms.

A more detailed comparison of the decay kinetics of spIPSCs and the deactivation kinetics of patch responses evoked by brief pulses of glycine suggests that the synaptic receptors and the extrasynaptic receptors are similar, but not identical (Table 1). Both τ_{fast} and, in particular, τ_{slow} were longer for the patch responses than for the spIPSCs. This could be due to differences in the exact subunit composition of synaptic *versus* extrasynaptic receptors or differences in the modulatory state of specific subunits. The decay kinetics of glycinergic spIPSCs and the deactivation kinetics of glycine responses in patches were considerably slower for wide-field amacrine cells than for AII amacrine cells (Table 1; Gill *et al.* 2006). We are aware of only one other report that has measured kinetic properties of glycinergic spIPSCs in mammalian amacrine cells. Frech *et al.* (2001) recorded glycinergic spIPSCs in four unidentified mouse amacrine cells and reported a decay time constant of 25 ms. It is unclear, however, if the decay was best fitted by a single- or double-exponential function.

Non-stationary noise analysis of spIPSCs and patch responses in wide-field amacrine cells yielded an average apparent single-channel conductance of 34 pS and 31 pS, respectively. With an average spIPSC peak amplitude of ~23 pA, this corresponds to ~11 glycine receptor channels being open at the peak of a single spIPSC. With a saturating concentration of agonist, the glycine receptors in patches reached a maximum P_{open} of 0.76. If the synaptic receptors reach a similar maximum P_{open}, these estimates suggest that 14–15 receptors are available to bind transmitter after release of a single vesicle.

Glycine receptors expressed by wide-field amacrine cells

Individual estimates of glycine receptor single-channel conductance by non-stationary noise analysis ranged from 24 pS to 48 pS for spIPSCs and from 19 pS to 39 pS for patches. We directly identified single-channel transitions between closed and open states in both types of responses. For patch responses, we observed openings corresponding to a single-channel conductance of ~47 pS (42–52 pS) in 11/11 patches. In addition, we observed conductance levels at 25–28 pS, 32–38 pS and 70–83 pS, but none at 100–110 pS. The multiple conductance levels could reflect a corresponding receptor heterogeneity, but could also be related to the documented presence of subconductance levels of glycine receptors in the outside-out patch configuration (Bormann *et al.* 1987; Takahashi & Momiyama, 1991; Beato & Sivilotti, 2007). For spIPSCs, the signal-to-noise ratio was lower, but we could directly identify openings with a single-channel conductance of ~35 pS and ~47 pS. Given that the directly resolved channel openings were observed during later phases of the responses, it is possible that additional conductance levels remained undetected if the corresponding channels displayed faster decay kinetics and thereby contributed primarily to the peak of the response.

The slow decay kinetics of spIPSCs and patch responses suggest that the α2-glycine receptor subunit contributes to both synaptic and extrasynaptic receptors in wide-field amacrine cells (Takahashi & Momiyama, 1991). In immunocytochemical studies of the distribution of glycine receptor subunits in mouse retina (Haverkamp *et al.* 2003, 2004), many α2- and α3-immunoreactive clusters were found in register with amacrine cell processes labelled for the GABA-synthesizing enzyme glutamic acid decarboxylase (GAD). Because wide-field amacrine cells presumably are GABAergic (Pourcho & Goebel, 1983; reviewed by Vaney, 1990), this suggests that these and other GABAergic amacrine cells receive glycinergic synaptic input mediated via receptors containing these subunits. At the same time, it is difficult to exclude a contribution of receptors with the kinetically faster α1-subunit to wide-field amacrine cells, particularly for synaptic receptors which displayed faster decay kinetics than extrasynaptic receptors (see above). Notably, in a study of glycine receptors in zebrafish embryos, Ali *et al.* (2000) demonstrated that simulations of evoked currents with varying relative proportions of glycine receptors with slow ('α2') and fast ('α1') decay kinetics resulted in responses with intermediate decay kinetics. On the average, the decay kinetics of glycinergic spIPSCs in wide-field amacrine cells are most similar to glycinergic spIPSCs of 'intermediate' kinetics in zebrafish embryos (Ali *et al.* 2000). Both types of spIPSCs displayed faster decay kinetics than 'slow' spIPSCs in zebrafish embryos. On the other hand, the decay kinetics of glycine-evoked patch responses in wide-field amacrine cells are most similar to the decay kinetics of 'slow' patches in zebrafish embryos, and, to our knowledge, these are the slowest responses reported for glycine receptors. Both spIPSCs

and patch responses in wide-field amacrine cells display slower decay kinetics than spIPSCs and patch responses in neonatal brain stem motoneurons where the $\alpha 2$-subunit is thought to be involved (Singer *et al.* 1998; Singer & Berger, 1999). We are not aware of any reports that have measured deactivation kinetics of responses mediated by receptors involving the $\alpha 3$- and $\alpha 4$-subunits. Accordingly, the possibility that these subunits are expressed by the wide-field amacrine cells we have recorded from and contribute to their spIPSCs has to be kept open.

A single-channel conductance of ∼47 pS, as observed in both spIPSCs and in patch responses, suggests the presence of heteromeric $\alpha\beta$ receptors (44–54 pS; Bormann *et al.* 1993), as opposed to homomeric receptors. Previous evidence has suggested the presence of homomeric receptors in extrasynaptic, but not synaptic glycine receptors (Takahashi *et al.* 1992). The lack of single-channel openings at the level characteristic of homomeric $\alpha 2$ receptors (100–110 pS; Bormann *et al.* 1993) suggests the absence of such receptors in these cells. This is consistent with evidence that the specific properties of homomeric $\alpha 2$ receptors impairs a proper synaptic functioning (Mangin *et al.* 2003), in particular the low P_{open} attained at transmitter concentrations thought to be reached in the synaptic cleft (1–3 mM). In patches from wide-field amacrine cells we found an average peak P_{open} of 0.76 with 3 mM glycine. We are not aware of any reports that have measured P_{open} for $\alpha 2\beta$ heteromeric receptors. On the basis of these observations, and assuming that $\alpha 2$ receptor subunits contribute to the synaptic glycine receptors of the wide-field amacrine cells studied here, we propose that the receptors are dominated by heteromeric $\alpha 2\beta$, as opposed to homomeric $\alpha 2$, receptors. Because the apparent single-channel conductance estimates (for both spIPSCs and patches) are lower than the presumed main conductance state for heteromeric receptors (∼47 pS), it is likely that lower conductance states make a significant contribution to glycine-evoked activity.

Functional consequences of the kinetic properties of glycine receptor channels in wide-field amacrine cells

The slow decay kinetics of spIPSCs in wide-field amacrine cells will impact the integrative properties of these cells and determine how inhibitory inputs shape their response properties. With perfectly synchronous release, the slow kinetics of spIPSCs set a lower limit on the time course of evoked IPSCs. This means that summation of input will occur at relatively low input frequencies, and that wide-field amacrine cells might be effective integrators of glycinergic input. Without knowledge of the activity patterns of their presynaptic inputs, the potential physiological relevance is difficult to predict. Another implication is that the timing of the inhibitory input, relative to that of the excitatory input, may not be very critical for the functional impact of glycinergic inhibition in several types of wide-field amacrine cells. If inhibitory input to wide-field amacrine cells primarily acts as shunting inhibition, the long duration of glycinergic synaptic events will lead to a correspondingly long-lasting inhibition. It will therefore be important to investigate the kinetic properties of the receptors mediating glutamatergic input from bipolar cells to wide-field amacrine cells.

For wide-field amacrine cells in rat retina, we are not aware of previous morphological or physiological studies that have directly addressed the type(s) of cells we have recorded from. In general, however, electron microscopic investigations have revealed that the dendrities of wide-field amacrine cells typically are both presynaptic (with synaptic vesicles) as well as postsynaptic (with corresponding membrane specializations) (Dowling & Boycott, 1965). Because of the proximity of pre- and postsynaptic sites along the dendrites of many wide-field amacrine cells, it is likely that local glycinergic, inhibitory input will directly modulate transmitter release from neighbouring presynaptic sites. In the thin dendritic processes of these cells, the input resistance is likely to be high such that small excitatory synaptic currents can give rise to relatively large depolarizations, amplified by activation of voltage-gated currents (Koizumi *et al.* 2001). The long-lasting glycinergic inhibition observed here could be a very effective mechanism for counteracting activation of these voltage-gated currents. For rat amacrine cells in culture, there is evidence that propagating action potentials can be generated both locally in dendritic regions as well as in the soma (Koizumi *et al.* 2001), and that propagation from the soma to individual dendrites can be regulated by inhibitory input (Yamada *et al.* 2002). If similar mechanisms operate in wide-field amacrine cells *in vivo*, it is tempting to speculate that the glycinergic inhibitory input we have observed in the present study could be involved in dynamic regulation of the output characteristics of these cells. In wide-field amacrine cells of tiger salamander retina, there is physiological evidence that excitatory input from bipolar cells is concentrated to a narrow area of processes close to the soma, while inhibitory input is distributed over a larger area of the dendritic tree (Cook & Werblin, 1994). Similar mapping of the spatial sensitivity to excitatory and inhibitory transmitters of wide-field amacrine cells in the mammalian retina remains to be performed. In light of the slow decay kinetics of the glycinergic IPSCs observed in the wide-field amacrine cells and the location of their dendritic processes in a specific stratum of the inner plexiform layer, it is also possible that some types of wide-field amacrine cells, and their presynaptic glycinergic partners, could be involved in a disinhibitory circuit with operational characteristics similar to those proposed to generate transient visual responses of ganglion cells in the amphibian retina (Roska *et al.* 1998).

Of the glycinergic amacrine cells described in the rat retina (Menger *et al.* 1998), all are narrow-field cells. Some have dendritic trees restricted to the OFF-sublamina, some have dendritic trees restricted to the ON-sublamina, and others have dendritic trees spanning both the ON- and OFF-sublamina. In addition, the processes of all glycinergic amacrine cells span at least two strata of the inner plexiform layer. Thus, the narrow stratification of wide-field amacrine cells, like the ones studied here, is not matched by a correspondingly narrow stratification of potential candidates for glycinergic input. The morphology of the dendritic trees of glycinergic amacrine cells suggests that these cells have the potential to communicate between different strata and sublaminae (ON *versus* OFF) of the inner plexiform layer (reviewed by Wässle, 2004), and also means that we cannot predict the visual response polarity (OFF *versus* ON *versus* ON/OFF) of the glycinergic input to wide-field amacrine cells stratifying at a specific level of the inner plexiform layer.

References

Ali DW, Drapeau P & Legendre P (2000). Development of spontaneous glycinergic currents in the Mauthner neuron of the zebrafish embryo. *J Neurophysiol* **84**, 1726–1736.

Baccus SA (2007). Timing and computation in inner retinal circuitry. *Annu Rev Physiol* **69**, 271–290.

Badea TC & Nathans J (2004). Quantitative analysis of neuronal morphologies in the mouse retina visualized by using a genetically directed reporter. *J Comp Neurol* **480**, 331–351.

Beato M & Sivilotti LG (2007). Single-channel properties of glycine receptors of juvenile rat spinal motoneurones *in vitro*. *J Physiol* **580**, 497–506.

Becker CM, Hoch W & Betz H (1988). Glycine receptor heterogeneity in rat spinal cord during postnatal development. *EMBO J* **7**, 3717–3726.

Bormann J, Hamill OP & Sakmann B (1987). Mechanism of anion permeation through channels gated by glycine and γ-aminobutyric acid in mouse cultured spinal neurones. *J Physiol* **385**, 243–286.

Bormann J, Rundström, Betz H & Langosch D (1993). Residues within transmembrane segment M2 determine chloride conductance of glycine receptor homo- and hetero-oligomers. *EMBO J* **12**, 3729–3737.

Cook PB & Werblin FS (1994). Spike initiation and propagation in wide field transient amacrine cells of the salamander retina. *J Neurosci* **14**, 3852–3861.

Cui J, Ma Y-P, Lipton SA & Pan Z-H (2003). Glycine receptors and glycinergic synaptic input at the axon terminals of mammalian retinal rod bipolar cells. *J Physiol* **553**, 895–909.

Cull-Candy SG, Howe JR & Ogden DC (1988). Noise and single channels activated by excitatory amino acids in rat cerebellar granule neurones. *J Physiol* **400**, 189–222.

Dowling JE & Boycott BB (1965). Neural connections of the retina: fine structure of the inner plexiform layer. *Cold Spring Harb Symp Quant Biol* **30**, 393–402.

Famiglietti EV (1992*a*). Polyaxonal amacrine cells of rabbit retina: morphology and stratification of PA1 cells. *J Comp Neurol* **316**, 391–405.

Famiglietti EV (1992*b*). Polyaxonal amacrine cells of rabbit retina: PA2, PA3, and PA4 cells. Light and electron microscopic studies with a functional interpretation. *J Comp Neurol* **316**, 422–446.

Frech MJ, Pèrez-León J, Wässle H & Backus KH (2001). Characterization of the spontaneous synaptic activity of amacrine cells in the mouse retina. *J Neurophysiol* **86**, 1632–1643.

Gill SB, Veruki ML & Hartveit E (2006). Functional properties of spontaneous IPSCs and glycine receptors in rod amacrine (AII) cells in the rat retina. *J Physiol* **575**, 739–759.

Grünert U & Wässle H (1993). Immunocytochemical localization of glycine receptors in the mammalian retina. *J Comp Neurol* **335**, 523–537.

Hartveit E (1996). Membrane currents evoked by ionotropic glutamate receptor agonists in rod bipolar cells in the rat retinal slice preparation. *J Neurophysiol* **76**, 401–422.

Hartveit E & Veruki ML (2006). Studying properties of neurotransmitter receptors by non-stationary noise analysis of spontaneous synaptic currents. *J Physiol* **574**, 751–785.

Harvey RJ, Schmieden V, von Holst A, Laube B, Rohrer H & Betz H (2000). Glycine receptors containing the α4 subunit in the embryonic sympathetic nervous system, spinal cord and male genital ridge. *Eur J Neurosci* **12**, 994–1001.

Haverkamp SM, Müller U, Harvey K, Harvey RJ, Betz H & Wässle H (2003). Diversity of glycine receptors in the mouse retina: localization of the α3 subunit. *J Comp Neurol* **465**, 524–539.

Haverkamp SM, Müller U, Zeilhofer HU, Harvey RJ & Wässle H (2004). Diversity of glycine receptors in the mouse retina: localization of the α2 subunit. *J Comp Neurol* **477**, 399–411.

Heinemann SH & Conti F (1992). Nonstationary noise analysis and application to patch clamp recordings. *Meth Enzymol* **207**, 131–148.

Heinze L, Harvey RJ, Haverkamp S & Wässle H (2006). Diversity of glycine receptors in the mouse retina: localization of the α4 subunit. *J Comp Neurol* **500**, 693–707.

Ivanova E, Müller U & Wässle H (2006). Characterization of the glycinergic input to bipolar cells of the mouse retina. *Eur J Neurosci* **23**, 350–364.

Jonas P (1995). Fast application of agonists to isolated membrane patches. In *Single-Channel Recording*, 2nd edn, ed. Sakmann B & Neher E, pp. 231–243. Plenum Press, New York.

Jonas P, Bischofberger J & Sandkühler J (1998). Corelease of two fast neurotransmitters at a central synapse. *Science* **281**, 419–424.

Koizumi A, Watanabe S-I & Kaneko A (2001). Persistent Na^+ current and Ca^{2+} current boost graded depolarization of rat retinal amacrine cells in culture. *J Neurophysiol* **86**, 1006–1016.

Legendre P (1998). A reluctant gating mode of glycine receptor channels determines the time course of inhibitory miniature synaptic events in zebrafish hindbrain neurons. *J Neurosci* **18**, 2856–2870.

Legendre P (2001). The glycinergic inhibitory synapse. *Cell Mol Life Sci* **58**, 760–793.

Lin B & Masland RH (2006). Populations of wide-field amacrine cells in the mouse retina. *J Comp Neurol* **499**, 797–809.

Lynch JW (2004). Molecular structure and function of the glycine receptor chloride channel. *Physiol Rev* **84**, 1051–1095.

MacNeil MA, Heussy JK, Dacheux RF, Raviola E & Masland RH (1999). The shapes and numbers of amacrine cells: matching of photofilled with Golgi-stained cells in the rabbit retina and comparison with other mammalian species. *J Comp Neurol* **413**, 305–326.

MacNeil MA & Masland RH (1998). Extreme diversity among amacrine cells: implications for function. *Neuron* **20**, 971–982.

Malosio ML, Marqueze-Pouey B, Kuhse J & Betz H (1991). Widespread expression of glycine receptor subunit mRNAs in the adult and developing rat brain. *EMBO J* **10**, 2401–2409.

Mangin JM, Baloul M, de Carvalho LP, Rogister B, Rigo JM & Legendre P (2003). Kinetic properties of the α_2 homo-oligomeric glycine receptor impairs a proper synaptic functioning. *J Physiol* **553**, 369–386.

Masland RH (2001). Neuronal diversity in the retina. *Curr Opinion Neurobiol* **11**, 431–436.

Menger N, Pow DV & Wässle H (1998). Glycinergic amacrine cells of the rat retina. *J Comp Neurol* **401**, 34–46.

Momiyama A, Silver RA, Häusser M, Notomi T, Wu Y, Shigemoto R & Cull-Candy SG (2003). The density of AMPA receptors activated by a transmitter quantum at the climbing fibre–Purkinje cell synapse in immature rats. *J Physiol* **549**, 75–92.

Mørkve SH, Veruki ML & Hartveit E (2002). Functional characteristics of non-NMDA-type ionotropic glutamate receptor channels in AII amacrine cells in rat retina. *J Physiol* **542**, 147–165.

Perry VH & Walker M (1980). Amacrine cells, displaced amacrine cells and interplexiform cells in the retina of the rat. *Proc R Soc Lond B Biol Sci* **208**, 415–431.

Pourcho RG & Goebel DJ (1983). Neuronal subpopulations in cat retina which accumulate the GABA agonist, (^{3}H)muscimol: a combined Golgi and autoradiographic study. *J Comp Neurol* **219**, 25–35.

Pourcho RG & Goebel DJ (1985). A combined Golgi and autoradiographic study of (^{3}H)glycine-accumulating amacrine cells in the cat retina. *J Comp Neurol* **233**, 473–480.

Protti DA, Gerschenfeld HM & Llano I (1997). GABAergic and glycinergic IPSCs in ganglion cells of rat retinal slices. *J Neurosci* **17**, 6075–6085.

Roska B, Nemeth E & Werblin FS (1998). Response to change is facilitated by a three-neuron disinhibitory pathway in the tiger salamander retina. *J Neurosci* **18**, 3451–3459.

Sigworth FJ (1980). The variance of sodium current fluctuations at the node of Ranvier. *J Physiol* **307**, 97–129.

Singer JH & Berger AJ (1999). Contribution of single-channel properties to the time course and amplitude variance of quantal glycine currents recorded in rat motoneurons. *J Neurophysiol* **81**, 1608–1616.

Singer JH, Talley EM, Bayliss DA & Berger AJ (1998). Development of glycinergic synaptic transmission to rat brain stem motoneurons. *J Neurophysiol* **80**, 2608–2620.

Slaughter MM (2004). Inhibition in the retina. In *The Visual Neurosciences*, ed. Chalupa LM & Werner JS, vol. 1, pp. 355–368. MIT Press, Cambridge, London.

Takahashi T (2005). Postsynaptic receptor mechanisms underlying developmental speeding of synaptic transmission. *Neurosci Res* **53**, 229–240.

Takahashi T & Momiyama A (1991). Single-channel currents underlying glycinergic inhibitory postsynaptic responses in spinal neurons. *Neuron* **7**, 965–969.

Takahashi T, Momiyama A, Hirai K, Hishinuma F & Akagi H (1992). Functional correlation of fetal and adult forms of glycine receptors with developmental changes in inhibitory synaptic receptor channels. *Neuron* **9**, 1155–1161.

Tian N, Hwang TN & Copenhagen DR (1998). Analysis of excitatory and inhibitory spontaneous synaptic activity in mouse retinal ganglion cells. *J Neurophysiol* **80**, 1327–1340.

Traynelis SF, Silver RA & Cull-Candy SG (1993). Estimated conductance of glutamate receptor channels activated during EPSCs at the cerebellar mossy fiber–granule cell synapse. *Neuron* **11**, 279–289.

Vaney DI (1990). The mosaic of amacrine cells in the mammalian retina. *Prog Ret Res* **9**, 49–100.

Veruki ML, Mørkve SH & Hartveit E (2003). Functional properties of spontaneous EPSCs and non-NMDA receptors in rod amacrine (AII) cells in rat retina. *J Physiol* **549**, 759–774.

Völgyi B, Xin D, Amarillo Y & Bloomfield SA (2001). Morphology and physiology of the polyaxonal amacrine cells in the rabbit retina. *J Comp Neurol* **440**, 109–125.

Wang P & Slaughter MM (2005). Effects of GABA receptor antagonists on retinal glycine receptors and on homomeric glycine receptor alpha subunits. *J Neurophysiol* **93**, 3120–3126.

Wässle H (2004). Parallel processing in the mammalian retina. *Nat Rev Neurosci* **5**, 747–757.

Yamada Y, Koizumi A, Iwasaki E, Watanabe S-I & Kaneko A (2002). Propagation of action potentials from the soma to individual dendrite of cultured rat amacrine cells is regulated by local GABA input. *J Neurophysiol* **87**, 2858–2866.

Acknowledgements

Financial support from the Norwegian Research Council (NFR 161217/V40), the Meltzer fund (University of Bergen) and the Faculty of Medicine at the University of Bergen (fellowships for M.L.V. and S.B.G.) is gratefully acknowledged. S.B.G. is supported by the medical student research program ('Forskerlinje') of the Faculty of Medicine at the University of Bergen. We thank Dr Svein H. Mørkve for valuable advice on ultrafast drug application.